Applications in Energy and Combustion Science 12 (2022) 100095

Contents lists available at ScienceDirect

Applications in Energy and Combustion Science

journal homepage: www.elsevier.com/locate/jaecs

NH_3 oxidation by NO_2 in a jet-stirred reactor: The effect of significant uncertainties in H_2NO kinetics

Rodger E. Cornell [a,d], Mark C. Barbet [a], Joe Lee [a], Michael P. Burke [a,b,c,*]

[a] Department of Mechanical Engineering, Columbia University, NY 10027, United States
[b] Department of Chemical Engineering, Columbia University, NY 10027, United States
[c] Data Science Institute, Columbia University, NY 10027, United States
[d] US Army DEVCOM – Armaments Center, Detonation Physics and Experimental Research Branch, Picatinny Arsenal, NJ 07806, United States

ARTICLE INFO

Keywords:
Ammonia
Jet-stirred reactor
NO_x chemistry
Nitrogen kinetics

ABSTRACT

Understanding the kinetics of ammonia (NH_3) is becoming increasingly important to a growing variety of applications — ranging from its role as a NO_x reduction agent, a key intermediate during combustion of biomass and energetic materials (especially green propellants), and a potential carbon-free energy carrier and storage medium. This wide variety of applications calls for comprehensive NH_3 kinetic models that are reliable over wide ranges of temperatures, pressures, and mixtures. Yet, many still consider the present understanding of its kinetics to be incomplete. For example, there are few experimental studies of NH_3 oxidation by nitrogen-containing species, which offer the opportunity to probe relatively untested reactions (or combinations thereof) to enable a more comprehensive understanding of NH_3 kinetics. To address this gap, we perform jet-stirred reactor experiments of NH_3 oxidation by NO_2 over an intermediate temperature range (700–1100 K). The mole fractions of NH_3, NO_2, NO, and O_2 are measured through a combination of gas chromatography, chemiluminescence, and infrared absorption. Agreement among different diagnostics ($\leq$4% for NH_3 and $\leq$7% for NO_2) and excellent experimental repeatability ensure high confidence in all species measurements. Comparisons of species measurements to model predictions revealed deficiencies in recent kinetic models, particularly for NH_3 consumption and NO formation at elevated temperatures ($\geq$900 K). Uncertainty-weighted kinetic analyses point to the importance of reactions that form ($NH2 + NO_2$) and consume ($H_2NO + NO_2$, $H_2NO + OH$) H_2NO, both of which are uncertain and influential in this system (and many other NH_3 oxidation systems). These and other reactions accentuated in the present dataset are also key reactions in NH_3/air ignition and N_2O formation, both of which remain outstanding challenges for NH_3 combustion in engines. Consequently, resolving the modeling deficiencies observed for the present dataset appears especially important to predictive models to enable the use of NH_3 as a fuel.

1. Introduction

The kinetics of ammonia (NH_3) have been a topic of substantial (and rapidly growing) interest given its importance across many different scientific and engineering domains. Noteworthy examples of its relevance include its potential as a carbon-free energy carrier and/or storage medium [1–5], its continued use as a NO_x reduction agent during Thermal DeNO_x [6–12] and other similar processes [13], its presence as a major species during the decomposition of many energetic materials [14–22], its role as an important gasification impurity during biofuel and biomass combustion [23–26], and even its appearance in atmospheric chemistry [27], marine toxicity [28], and neurobiology [29]. Many recent studies are motivated by the potential use of NH_3 as a carbon-free fuel in combustion devices (e.g. internal combustion engines) [3,30–36].

With such far-reaching and varied applications, there is a need for comprehensive NH_3 oxidation models that can accurately predict kinetic behavior over a wide range of operational conditions. Despite extensive NH_3 experimental and modeling research efforts conducted over the last half century, many researchers still consider its kinetics to be incompletely understood. Stagni et al. note in their recent publication [37] that "a comprehensive understanding of its kinetic behavior is still an open challenge, especially at low-temperature (T< 1200 K) and under diluted conditions". In a similar vein, Cañas et al. [38] point out that "in spite of the efforts updating the ammonia oxidation models, the models are far from complete since not all combustion properties

* Corresponding author at: Department of Mechanical Engineering, Columbia University, NY 10027, United States.
E-mail address: mpburke@columbia.edu (M.P. Burke).

https://doi.org/10.1016/j.jaecs.2022.100095
Received 8 June 2022; Received in revised form 7 October 2022; Accepted 31 October 2022
Available online 8 November 2022

are described satisfactorily and consequently they are not completely accurate".

For example, our own survey of the literature over the last ~50 years has revealed that a majority of the NH_3 oxidation studies conducted have utilized molecular oxygen (O_2) as the primary oxidizer [8,35,38–45]. While trace amounts of nitrogen oxides (e.g. NO, NO_2, N_2O) are often included in Thermal $DeNO_x$ and solid fuel combustion studies [6,7,9,10,12,46–48], O_2 is still typically available in large mole fractions. Studies of NH_3 oxidation by nitrogen-containing species in the absence of O_2, however, are much more limited (e.g. [49]) and may provide insights into reactions that are highly uncertain due to a lack of supporting experimental and theoretical data.

Indeed, the results from our earlier work on NH_3 oxidation by N_2O in a jet-stirred reactor [26] revealed significant deficiencies in recent models — in terms of both untested reactions (e.g. NH_2 + N_2O) and untested combinations of reactions that were accentuated by NH_3 oxidation by nitrogen-containing oxidizers. Additionally, there are select combustion systems where NH_3 is more likely to be oxidized by nitrogen oxides (e.g. the combustion of energetic materials), making the results of such studies directly relevant to system kinetics.

Of particular interest here is the oxidation of NH_3 by NO_2. While NH_3 oxidation by NO_2 involves many of the same intermediate species as NH_3 oxidation by O_2, the NH_3/NO_2 system isolates reaction sequences that are usually intermixed with many other pathways when significant mole fractions of O_2 are present (e.g. compare the present jet-stirred reactor results below with those from [37]). For example, in the presence of large mole fractions of NO_2, NH_3 consumption is dominated by reaction with OH, whereas significant mole fractions of O_2 allow for NH_3 consumption by several reactions involving OH, O, and HO_2. Additionally, significant mole fractions of NO_2 emphasize NH_2 reactions with NO and NO_2, whereas significant mole fractions of O_2 also allow for NH_2 reactions with OH, O, and HO_2. Finally, when NO_2 is the primary oxidizer, H_2NO largely reacts with NO_2 and OH, whereas H_2NO also reacts with O_2 and/or HO_2 when significant mole fractions of O_2 are present.

For context, many of the abovementioned reactions isolated during NH_3 oxidation by NO_2 are of great importance to various combustion systems. In particular, the $NH_2 + NO_2$ reaction has significant influence over the reduction of NO, formation of N_2O during solid fuel combustion and ammonia combustion [2–4,50], and high-pressure ignition of NH_3 [37,51,52]; the NH_2 + NO reaction provides one of the key radical producing channels during applications of the Thermal $DeNO_x$ process [6,7,10,12,33]; and numerous reactions involving H_2NO impact high-pressure NH_3 ignition [37,51,52] and the mitigation of NO_x emissions from current and future NH_3-fueled combustion devices [4,30,31]. With such far-reaching and varied applications, any deficiencies in the rate constants of these reactions would be of significant interest to future NH_3 research and applications.

To address current gaps in experimental data and accentuate new combinations of rate constants, we present experimental data for NH_3 oxidation by NO_2 in a jet-stirred reactor at intermediate temperatures (700–1100 K) to assess the performance of recent kinetic models. Similar to our previous study on NH_3 oxidation by N_2O, comparison of the present experimental results and model predictions for NH_3 oxidation by NO_2 revealed significant discrepancies between experimental data and model predictions (and among model predictions themselves). Further modeling analyses point to the importance of reactions involving H_2NO that are both influential and highly uncertain and reveal several key reactions that are also influential to many NH_3 oxidation systems. Consequently, resolution of the observed discrepancies for NH_3 oxidation by NO_2 may be important to ensuring reliable predictions of NH_3 oxidation more generally.

Table 1
Experimental conditions with estimated uncertainties.

Mixture composition	214.8 ppm NH_3 (±2%) 197.4 ppm NO_2 (±2%) 396.0 ppm O_2 (±20%) balance N_2
Residence time	1.0 s (±5%)
Pressure	1.02 atm (±1%)
Temperature	700–1100 K (±1%)

2. Experimental methods

To quantitatively evaluate the NH_3/NO_2 kinetic system, experiments were performed for a reactant mixture of $NH_3/NO_2/O_2/N_2$ in the jet-stirred reactor (JSR) facility at Columbia University (Fig. 1) at the conditions specified in Table 1. The JSR facility consists of a flow delivery system that can prepare complex mixtures of multiple gases and liquids, an automated temperature control system capable of heating the reactor just beyond 1200 K, a JSR design found to promote rapid mixing in previous studies, and several online fast-response diagnostics that enable simultaneous measurements of multiple species. Of particular note is that all major components are computer controllable to enable later planned high-throughput and/or automated operation at experimental conditions selected by Bayesian Design of Experiments [53,54]. This JSR facility is described in further detail in our earlier work [26] and only key details pertaining to the present work are presented below.

Here, flow delivery was achieved through two Bronkhorst EL-FLOW Prestige mass flow controllers (MFCs) that control the flow rates of individual reactant components into a mixing manifold upstream of the reactor. Total volumetric flow rates controlled by the MFCs ranged from 1.27–2.00 L/min (with a ±1% uncertainty) to yield a constant nominal residence time inside the JSR of 1.0 s across all temperatures. To reduce reactant mixture composition uncertainties, two certified gas mixtures of NH_3/N_2 and $NO_2/O_2/N_2$, whose composition and specified uncertainties are provided in Table 1, were directly flowed from two independent MFCs. While the mole fractions of NH_3 and NO_2 were specified by the gas supplier in the certified NH_3/N_2 and $NO_2/O_2/N_2$ mixtures, respectively, the mole fraction of O_2, which was included in the certified $NO_2/O_2/N_2$ mixture to promote long-term stability of NO_2, was not specified by the gas supplier. As such, the mole fraction of O_2 reported in Table 1 reflects our own gas chromatography measurements. Similarly, our chemiluminescence measurements of trace amounts of NO also present in the certified $NO_2/O_2/N_2$ mixture indicated a mole fraction of ~0.5 ppm, which remained stable throughout all experiments (~6 months) and thereby confirmed the stability of the mixture. Simulations with and without these amounts of O_2 and NO in the reactant mixture are nearly indistinguishable (Figure S12 in the Supplemental Information), such that the presence of O_2 and NO in the reactant mixture appear to have no perceivable influence on system kinetics.

The quartz JSR is based on the design of Herbinet et al. [55,56], which has been found to closely mimic a perfectly-stirred reactor when operating within its intended range of conditions [57,58]. Prior to entering the JSR, all reactants are combined in a mixing manifold and flowed through an annular preheat zone that rapidly heats the mixture to the reactor temperature to maintain thermal homogeneity within the reactor [59]. (Of note, given that the preheat volume is less than a few percent of the reactor volume, negligible reaction is expected to occur in the preheat zone under the present conditions — as supported by separate simulations that consider this additional residence time.) The preheated reactants are then ejected into the spherical reactor (56 mm inner diameter) through four quartz nozzles (0.25–0.30 mm inner diameter) positioned near the center of the reactor in a crossed configuration angled ~45° from the equatorial plane. The nominal

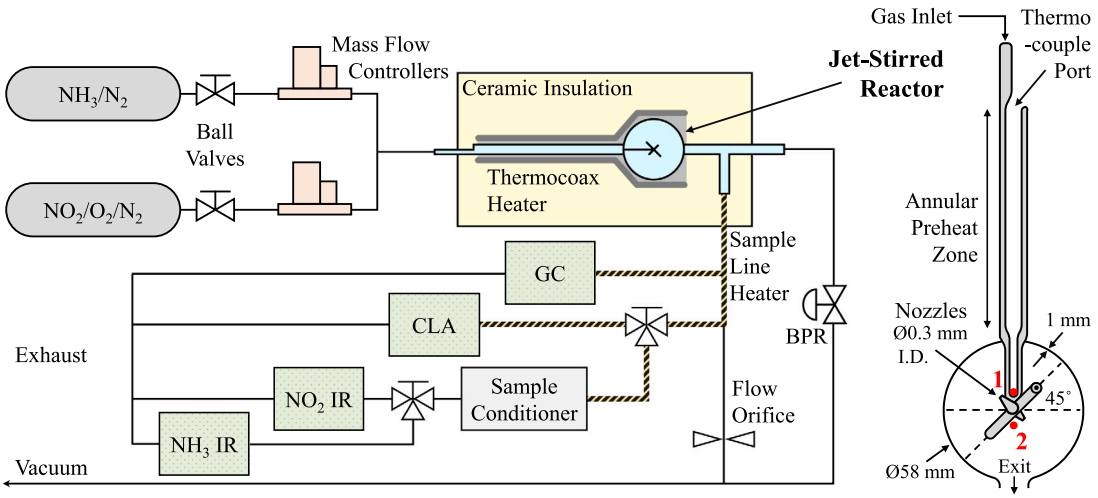

Fig. 1. A simplified schematic of the atmospheric-pressure jet-stirred reactor system used for this study (located at Columbia University). Thermocouple locations (1, 2) are shown in the magnified JSR image on the right side of the figure. Note that two MFCs were used for this study given that two certified standard gas tanks contained all reactant mixture components.

Table 2
Measurement uncertainties specific to each diagnostic instrument.

Observable	NH_3[a]	NH_3[b]	NO_2[a]	NO_2[b]	NO[a]	O_2[c]
Calibration	214.8 ppm ±2%	214.8 ppm ±2%	197.4 ppm ±2%	197.4 ppm ±2%	196.0 ppm ±2%	multi-point
Drift	±2.5%	±3%	±1.5%	±1%	±1.5%	–
Linearity	±1%	±3%	±1%	±3%	±1%	–
Noise (1σ)	±7[d]/1[e]%	±2%	±7[d]/1[e]%	±1%	±0.5%	±4%
Resolution	25 ppb	1 ppm	25 ppb	1 ppm	25 ppb	20 ppm

[a]Chemiluminescence.
[b]Infrared absorption.
[c]Gas chromatography.
[d]Dilute sample (NH_3, NO_2).
[e]Non-dilute sample (NH_3+NO_2).

residence time provided in Table 1 is calculated by dividing the reactor volume (82 ± 2 cm^3 [26]) by the volumetric flow rate inside the reactor. Altogether, considering the uncertainty contributions from the reactor volume and volumetric flow rates, the estimated uncertainty in the 1.0 s nominal residence time is approximately ±5%.

The reactor temperature is maintained by an Thermocoax resistive heating element coupled to a Digi-Sense temperature controller that monitors temperature in the reactor at two locations (labeled '1' and '2' in Fig. 1) using independent Omega high-temperature, low-drift K-type thermocouple probes (SCAXL-062) that are rated to have ≤ ±1.5 K noise, ≤ ±1.5 K deviations from linearity, and ≤ ±2.8 K calibration drift. Limited testing in Ar has indicated spatial temperature variations within the reactor limited to ≤ ±5 K for temperatures of 700–1180 K [26] . Furthermore, the present low reactant mole fractions limit reaction exothermicity and, therefore, introduce negligible deviations to spatial temperature homogeneity in the reactor (adiabatic simulations at the present conditions suggest a maximum temperature rise of 3 K). Altogether, the estimated uncertainty in reactor temperature is ~ ±1% of each temperature set point.

The reactor pressure is controlled by an Equilibar dome-loaded back pressure regulator in the reactor's exhaust line based on the voltage output signal from an Omega high-accuracy, digital pressure gauge (DPG409-030 A). Reactor pressure is intentionally maintained slightly above atmospheric pressure at 1.02 atm to inhibit N_2 and O_2 contamination from the surrounding air in the reactor and sample line. Prior experiments indicate typical variations of less than 0.0007 atm from the 1.02 atm set point. Other uncertainties include the specified noise (±0.0007 atm), accuracy (±0.0014 atm), and long-term stability (±0.0021 atm) of the pressure gauge, all of which add up to an estimated uncertainty in the reactor pressure of < ±1%.

Three independent diagnostics measure species mole fractions at each experimental condition in the exiting gas mixture carried by silica-coated stainless-steel tubes maintained near 385 K. An Eco Physics AG NO_x chemiluminescence analyzer (CLA) is used to provide measures of NO, NO_2, and NH_3. This analyzer contains two independent detection cells that can each measure up to 500 ppm NO with a 25 ppb minimum resolution. This instrument also contains NO_x and NO_x-amine converters that break down NO_x and NO_x+NH_3, respectively, to produce proportional mole fractions of NO for detection. Running the NO_x and NO_x-amine converters simultaneously in separate detection cells provides a measure of NH_3 equal to the difference between the two signals. The same procedure can be followed measuring NO and NO_x in separate detection cells to provide measures of NO_2. The NO_x-amine converter enables a maximum NH_3 measurement of 500 ppm while the NO_x converter is limited to a maximum NO_x measurement of 10 ppm. Separate testing (i.e. not involving heated reactor components) has shown that the NO_x converter has a conversion efficiency near ~100% while the NO_x-amine converter is notably less efficient at ~89%. Conversion efficiencies were rigorously tested (including across varied $NO/NO_2/NH_3$ mixtures to assess any potential nonlinear and/or cross-component effects) and accounted for in all NO_2 and NH_3 CLA measurements (and their associated uncertainties) provided herein.

An Infrared Industries IR-208 gas analyzer (IR) provides duplicate measurements of NO_2 and NH_3. An external sample pump provides the analyzer with a steady sample flow of ≥0.75 L/min needed for stable absorption signals. Similar to the CLA, the IR analyzer allows for maximum NH_3 and NO_2 measurements of 500 ppm with a larger minimum resolution of ~1 ppm.

An Inficon Micro GC Fusion gas analyzer (GC) is used to measure O_2 with a minimum resolution near 20 ppm and corresponding limited

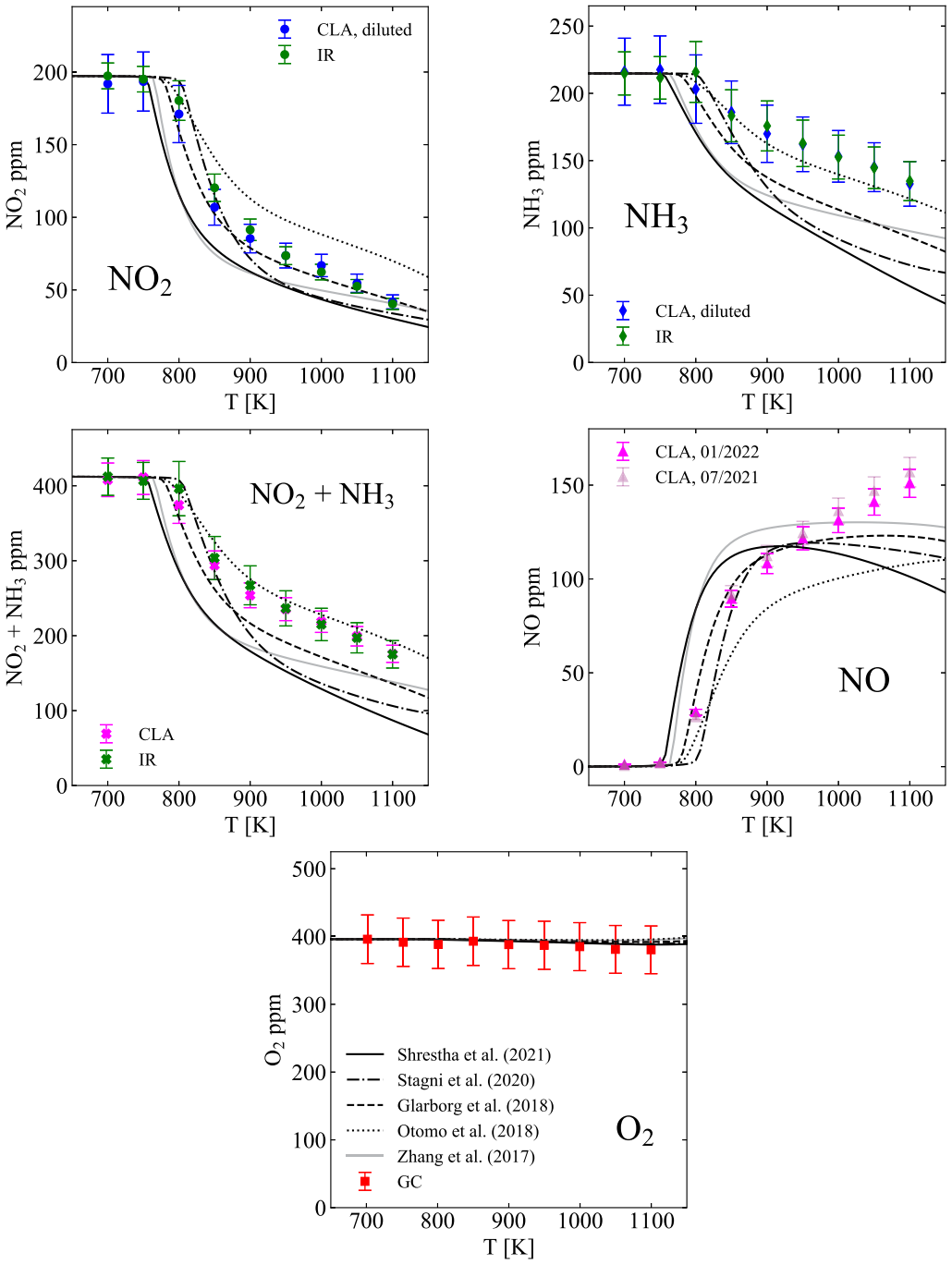

Fig. 2. Experimental measurements and model predictions [37,41,60–62] of NO_2, NH_3, NO_2+NH_3, NO, and O_2 for the conditions shown in Table 1.

capability below 100 ppm. While the GC is capable of measuring many other species, notably H_2 and N_2O, these molecules remain below or near detectable mole fraction limits over the experimental temperature range.

Species measurements are taken at every reactor temperature set point, which spanned from 700–1100 K in 50 K increments. All measurements are taken for a minimum of 10 min to ensure all wetted surfaces in the system and the detectors have adsorbed a sufficient amount of NH_3 so that its mole fraction remains stable [47,63]. After each measurement, all diagnostics are flushed with N_2 and re-calibrated using certified standard mixtures with specified uncertainties listed in Table 1 to limit NH_3 exposure and calibration drift, respectively. A multi-point calibration is performed for the GC measurements of O_2 over a mole fraction range that encompasses the full mole fraction range relevant to this study. For each diagnostic, the maximum observed signal drift and noise are reported in Table 2 for each measured species to bound their associated uncertainties. Additionally, calibration linearity is tested for each diagnostic and the corresponding uncertainties are reported in the same table. The uncertainties for each observable species for each diagnostic — the six columns of Table 2 — are summed independently at each temperature set point to produce the conservative error bar estimates provided in Fig. 2.

Given the limited range of the CLA NO_x converter (≤10 ppm), only the CLA NO_x-amine converter (≤500 ppm) is used to evaluate the reactant mixture of Table 1 and therefore can only provide a combined measurement of NO_2+NH_3. To measure NO_2 and NH_3 independently using the CLA, the sampled gaseous mixture exiting the

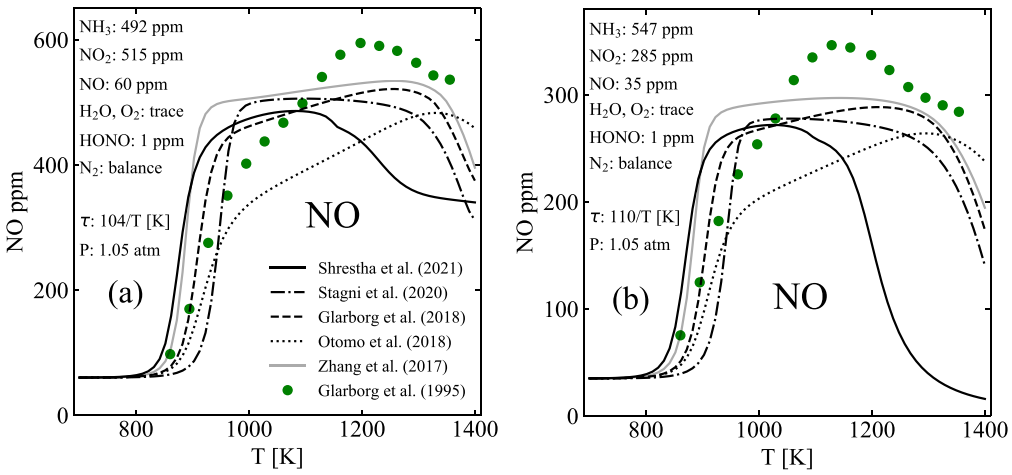

Fig. 3. Experimental measurements and model predictions of NO for flow reactor experiments performed by Glarborg et al. [49].

reactor is diluted with a known quantity of N_2 using a third MFC in a separate set of experiments. The sample is diluted by a factor of ~21 to reduce the combined NO_x signal ($NO+NO_2$) below 10 ppm over the experimental temperature range. This process enables independent measurements of NO_2 and NH_3 using the CLA (that are then scaled back to their undiluted values), but increases measurement uncertainty as a result of lower signal-to-noise ratios and added complications (with the corresponding increases in noise indicated in Table 2).

3. Kinetic simulation methods

The experiments described above are modeled using isothermal, isobaric, perfectly stirred reactor simulations performed in Cantera 2.4.059 [64] using an ideal gas equation of state and five recently developed kinetic models: the model of Zhang et al. [62], which focuses on hydrogen/syngas/NO_x kinetics but contains a recently updated H/N/O sub-mechanism; the model of Glarborg et al. [41], which includes a comprehensive treatment of nitrogen kinetics; and the ammonia oxidation models of Otomo et al. [61], Stagni et al. [37], and Shrestha et al. [60].

Each of these five kinetic models is also used to perform flux and kinetic sensitivity analyses for the NH_3/NO_2 system. For the uncertainty-weighted (u-w) kinetic sensitivity analyses, the most recently recommended uncertainty factors for each reaction among various rate constant evaluations [65–76] are used. A complete list of the uncertainty factors used here is provided in the Supplemental Information.

Simulations and equivalent flux analyses were also performed with modified versions of the same five kinetic models that employ recently published rate constants for $NH_2 + NO_2$ [77], $H_2NO + NO_2$ [78], and $H_2NO + OH$ [79] (as discussed further below).

4. Results and discussion

Experimental measurements and model predictions of NO_2, NH_3, NO, and O_2 are shown in Fig. 2. Measurements and predictions of NO_2+NH_3 are also provided as these CLA measurements are more direct and have lower uncertainty than the independent, diluted CLA measurements of NO_2 and NH_3. These CLA NO_2+NH_3 measurements are also compared to the sum of the IR NO_2 and NH_3 measurements.

The overall measurement consistency across diagnostics and experimental runs is very good with all measurements agreeing within their estimated uncertainties. Specifically, diluted CLA and IR measurements of NO_2 generally agree within 7% (aside from a slightly larger deviation at 850 K). Diluted CLA and IR measurements of NH_3 agree within 4% over the full temperature range. CLA and IR combined measurements of NO_2+NH_3 agree within 5% over the full temperature range. The two CLA NO measurement sets agree within 5% over the experimental temperature range — demonstrating the repeatability of the experimental results as these measurement sets were taken six months apart, during which time the CLA was serviced and cleaned. All measurements and predictions of O_2 agree within a few percent where the experiments and models agree that O_2 mole fractions remain stable over the temperature range.

The experimental measurements and model predictions for NO_2 and NH_3 agree qualitatively but noticeably differ quantitatively. While the model of Glarborg et al. [41] reproduces the NO_2 measurements and the model of Otomo et al. [61] reproduces the NH_3 measurements within estimated uncertainties, no model reproduces both NO_2 and NH_3 measurements — notably for NH_3, which is generally underpredicted by ~40%–80%. Experimental measurements and model predictions generally disagree both qualitatively and quantitatively for NO. The experimental measurements indicate a continued rise of the NO mole fraction with increasing temperature that is not reproduced by models except for that of Otomo et al. [61]. All models underpredict NO at higher temperatures — with deviations reaching ~20%–50% at 1100 K.

Interestingly, similar discrepancies between NO measurements and predictions are observed for the flow reactor experiments of NH_3 oxidation by NO_2 performed by Glarborg et al. [49] in 1995 (Fig. 3). The experimentally observed temperature dependence of the NO mole fraction is also not well captured by most models and measured peak NO mole fractions are under-predicted by a comparable margin (~20%–40%) using the same five models — suggesting that similar shortcomings in the kinetic models may be responsible for the discrepancies between NO predictions and measurements for both the flow reactor experiments of Glarborg et al. [49] and the jet-stirred reactor experiments presented here.

To better understand the observed discrepancies between experimental measurements and model predictions, flux analysis was performed at the experimental conditions listed in Table 1 using all five models. The results from this analysis are provided in Fig. 4 for the most influential species using the model from Glarborg et al. [41]. As evident from Fig. 4 and similar analyses using the other models [37,60–62] (Figures S6–S11 in the Supplemental Information), the reactions discussed below are found to be important for all models.

The results suggest that NH_3 (Fig. 2) is nearly exclusively consumed by bimolecular reactions with OH to form NH_2

$$NH_3 + OH \Leftrightarrow H_2O + NH_2 \quad \text{(R1)}$$

with a much smaller amount of NH_3 consumed by bimolecular reactions with NO_2

$$NH_3 + NO_2 \Leftrightarrow HONO + NH_2 \quad \text{(R2)}$$

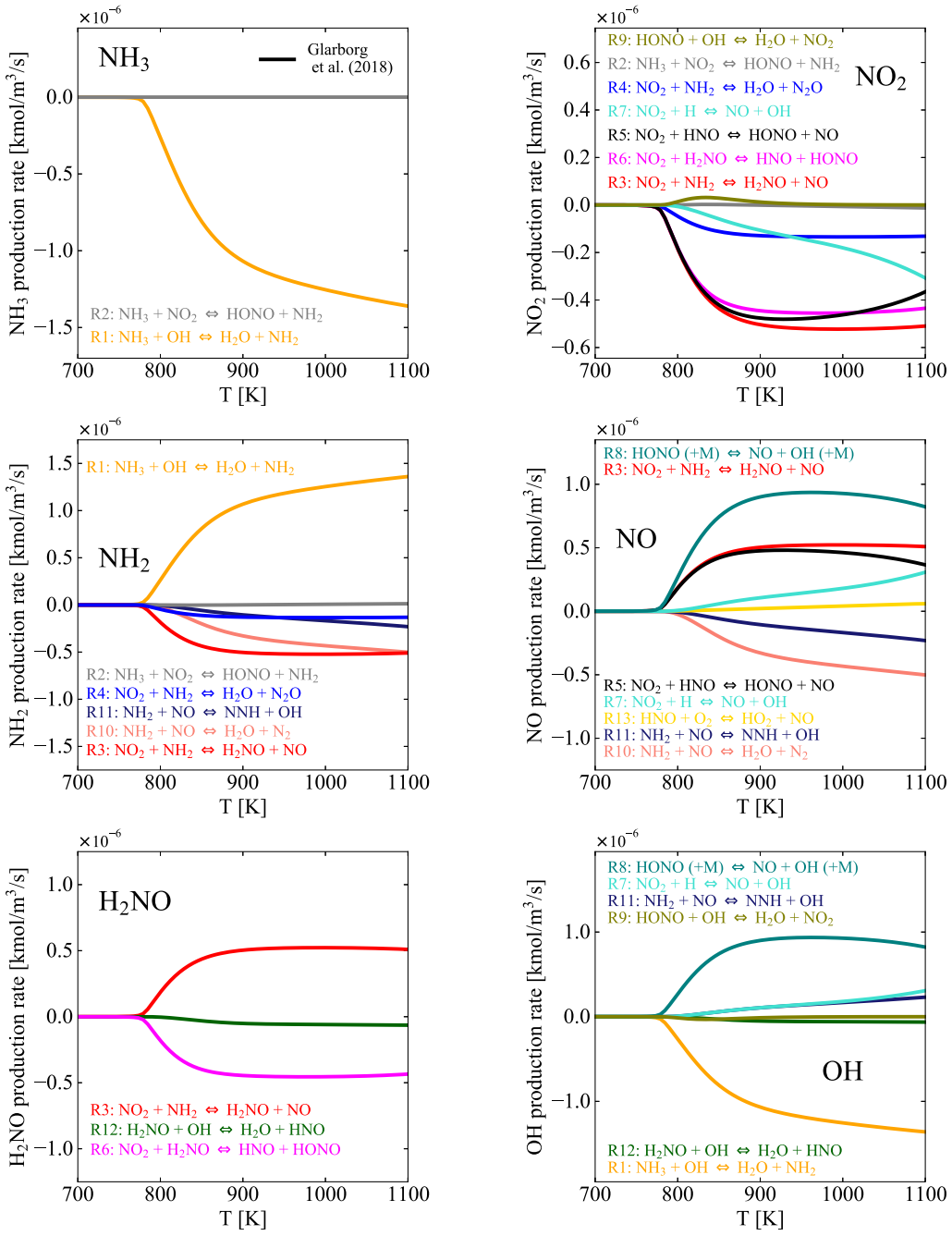

Fig. 4. Rate of production [kmol/m^3/s] of NH_3, NO_2, NH_2, NO, H_2NO, and OH generated using the model of Glarborg et al. [41].

which is also not a significant consumption route for NO_2. NO_2 is primarily consumed by bimolecular reactions with NH_2, HNO, and H_2NO at lower temperatures

$$NO_2 + NH_2 \Leftrightarrow H_2NO + NO \quad (R3)$$

$$NO_2 + NH_2 \Leftrightarrow H_2O + N_2O \quad (R4)$$

$$NO_2 + HNO \Leftrightarrow HONO + NO \quad (R5)$$

$$NO_2 + H_2NO \Leftrightarrow HNO + HONO \quad (R6)$$

and further consumed by bimolecular reactions with H at elevated temperatures

$$NO_2 + H \Leftrightarrow NO + OH \quad (R7)$$

OH is primarily produced by the unimolecular decomposition of HONO

$$HONO(+M) \Leftrightarrow NO + OH(+M) \quad (R8)$$

where HONO (not shown) is produced via (R2), (R5), and (R6), and partially consumed by bimolecular reactions with OH

$$HONO + OH \Leftrightarrow H_2O + NO_2 \quad (R9)$$

NH_2 is nearly exclusively produced from (R1) (and, to a lesser extent, (R2)) and consumed by bimolecular reactions with NO_2 ((R3), (R4)) and NO at elevated temperatures.

$$NH_2 + NO \Leftrightarrow H_2O + N_2 \quad (R10)$$

$$NH_2 + NO \Leftrightarrow NNH + OH \quad (R11)$$

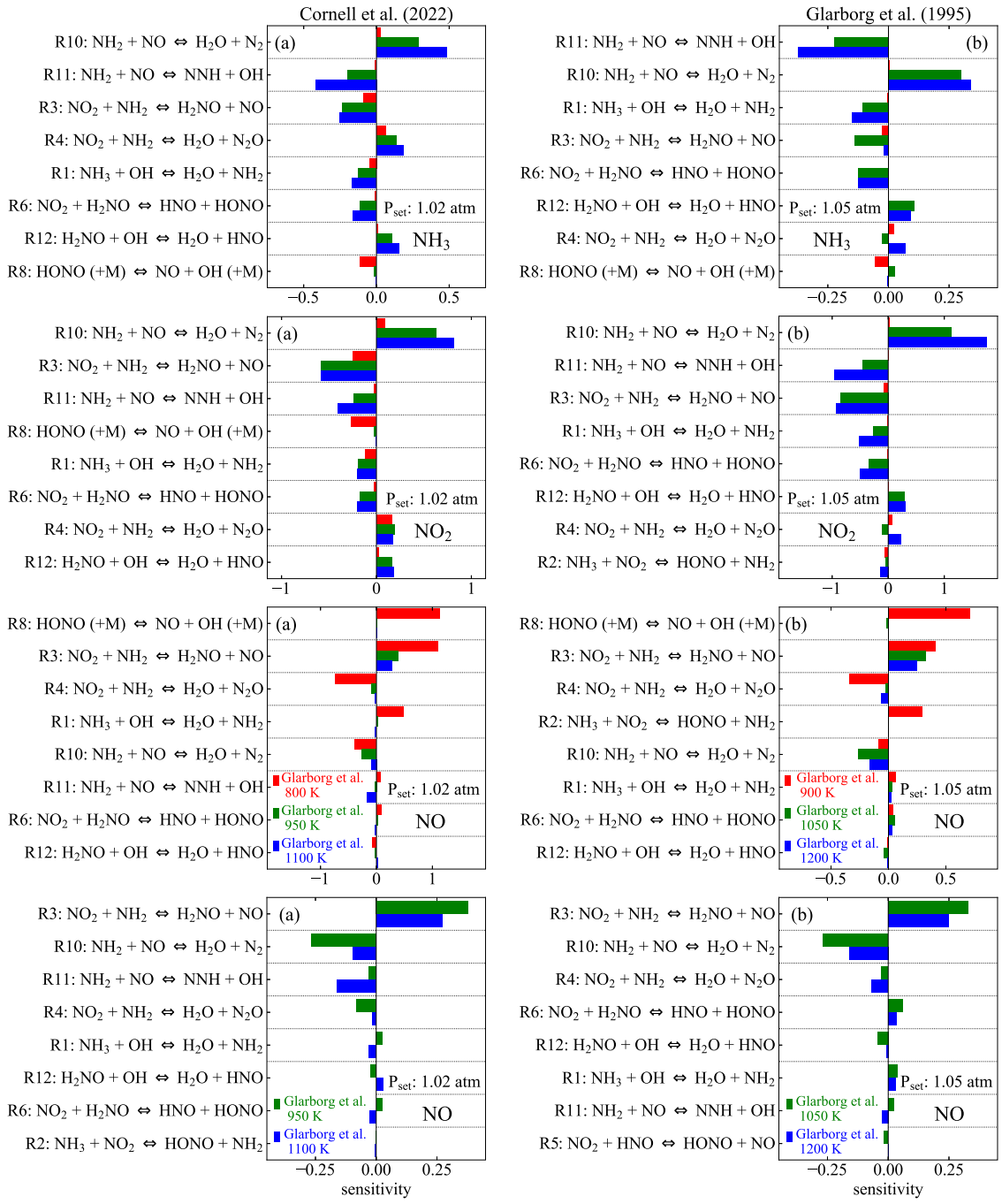

Fig. 5. Results from kinetic sensitivity analyses for NH_3, NO_2, and NO generated using the model of Glarborg et al. [41]. The left column (a) shows results for the present JSR experiments at 800 K (red), 950 K (green), and 1100 K (blue); the right column (b) shows results for the flow reactor experiments of Glarborg et al. [49] at 900 K (red), 1050 K (green), and 1200 K (blue). The NO results are presented in two sets of plots — including one without the lowest temperature to facilitate presentation of the results at higher temperatures, which have relatively lower sensitivity coefficients. (For interpretation of the references to color in this figure legend, the reader is referred to the web version of this article.)

HNO (not shown) is produced by (R6) and bimolecular reactions of H_2NO and OH

$$H_2NO + OH \Leftrightarrow H_2O + HNO \quad (R12)$$

and consumed by bimolecular reactions with NO_2 (R5) and O_2.

$$HNO + O_2 \Leftrightarrow HO_2 + NO \quad (R13)$$

While NO is primarily consumed by reactions with NH_2 ((R10), (R11)), NO is appreciably formed from several reactions, including (R3), (R5), (R8), and (R7).

Altogether, these results indicate that (R3), (R6), (R5), and (R8) in succession yields an overall chain-branching sequence

$$3NO_2 + NH_2 \Leftrightarrow 4NO + 2OH \quad (R14)$$

where radicals can also be diverted into chain-terminating pathways ((R4), (R10), (R12), and (R9)) that compete with each step of the chain-branching sequence. (There is also an alternative chain-branching sequence involving (R11), though this sequence is comparatively more minor in the present system).

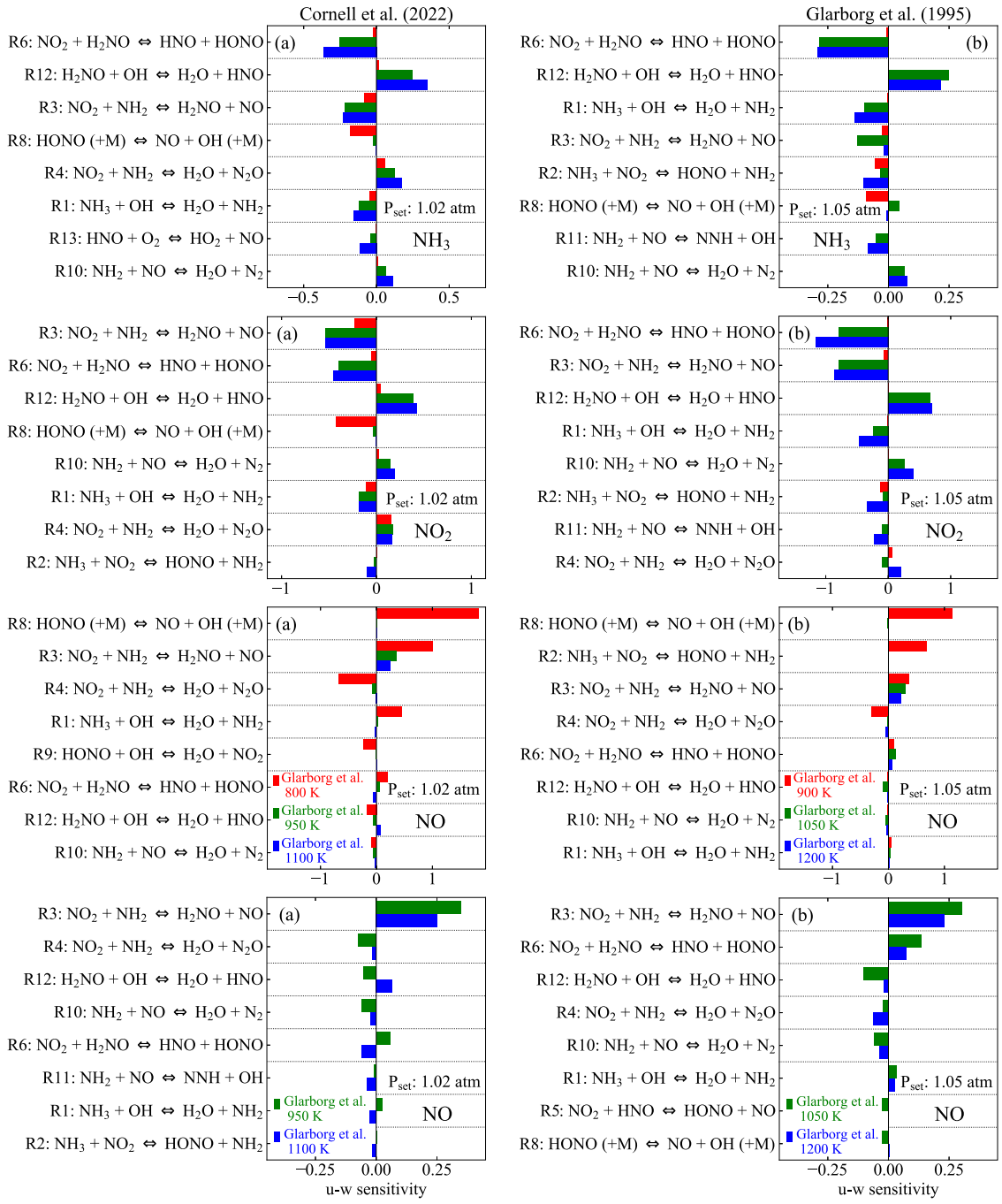

Fig. 6. Results from uncertainty-weighted (u-w) kinetic sensitivity analyses for NH_3, NO_2, and NO generated using the model of Glarborg et al. [41]. The left column (a) shows results for the present JSR experiments at 800 K (red), 950 K (green), and 1100 K (blue); the right column (b) shows results for the flow reactor experiments of Glarborg et al. [49] at 900 K (red), 1050 K (green), and 1200 K (blue). The NO results are presented in two sets of plots — including one without the lowest temperature to facilitate presentation of the results at higher temperatures, which have relatively lower sensitivity coefficients. (For interpretation of the references to color in this figure legend, the reader is referred to the web version of this article.)

To further explore possible sources of discrepancies between predictions and measurements, the sensitivities of the predicted mole fractions of species i to rate constants for each reaction j, $\partial\ln(X_i)/\partial\ln(k_j)$, were calculated for both the present JSR experiments and the flow reactor experiments of Glarborg et al. [49] at the conditions provided in Fig. 3a. The results of this analysis are shown in Fig. 5 for NH_3, NO_2, and NO using the model of Glarborg et al. [41] for the present JSR experiments (Fig. 5a) and flow reactor experiments of Glarborg et al. [49] (Fig. 5b). The results indicate that predictions of all three species are most sensitive to reactions (R3), (R4), (R10), and (R11) — which determine the fate of NH_2 and have differing implications for radical propagation — across the full temperature range of both experiments. Similarly, predictions of all three species are sensitive to the rate constants for (R6) and (R12) — which determine the fate of H_2NO and also have differing implications for radical propagation. As (R1) is primarily responsible for consuming NH_3 and OH and producing NH_2 to initiate the reaction sequence, it too influences predictions of all three species (NH_3, NO_2, NO). (R8) [80–85] is also influential, but only at lower temperatures near 800 K where all five models reasonably reproduce the observed onset of reaction. Reactions (R2) [86–88], (R5) [49,89–92], (R7) [75,93–95], (R9) [92,96], and (R13) [97] have limited influence on predicted mole fractions of NH_3, NO_2, and NO.

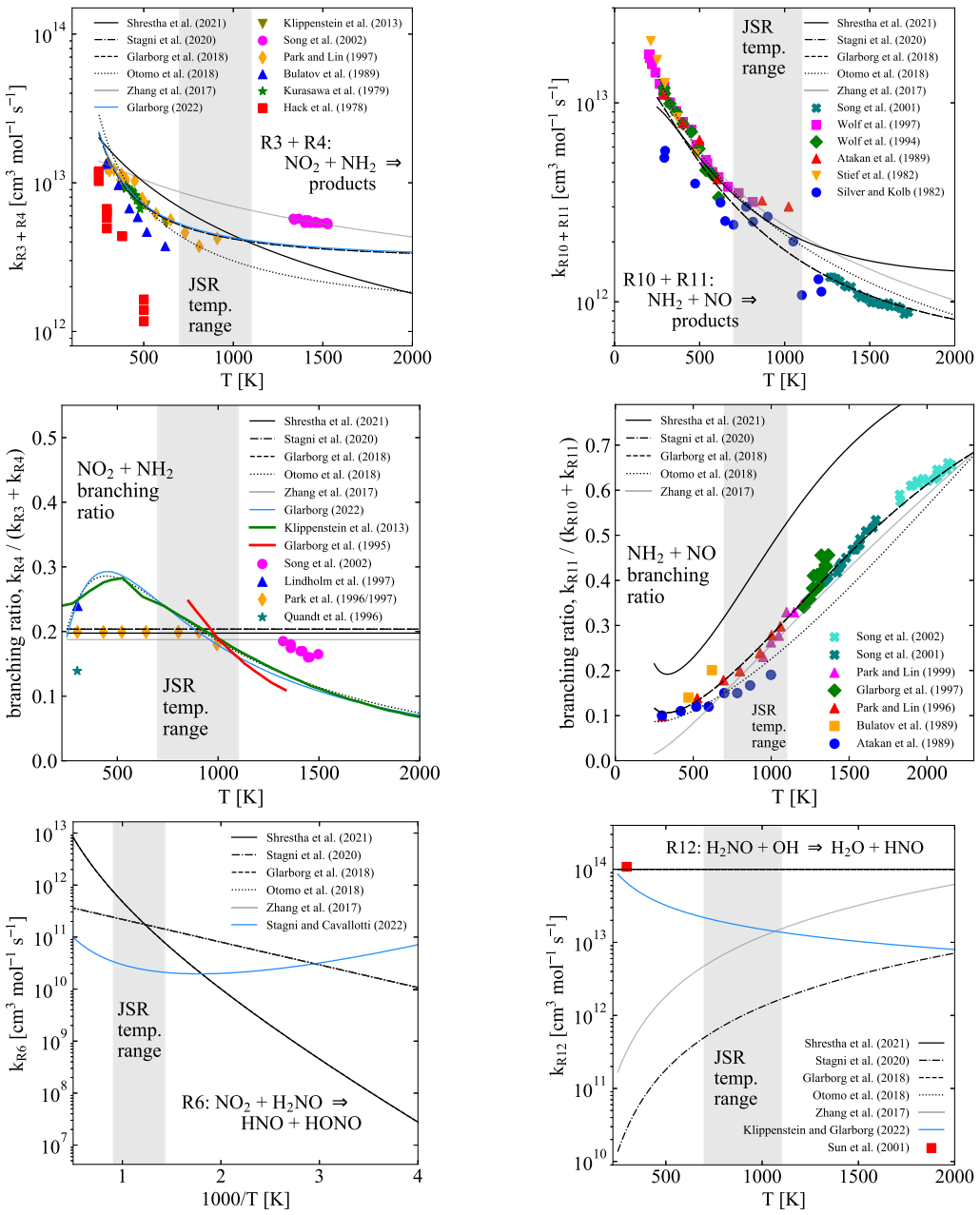

Fig. 7. Comparison of rate constants from the five models [37,41,60–62] with rate constants from theoretical calculations and experimental determinations for reactions (R3)+(R4), (R10)+(R11), (R6), and (R12). Branching ratios are also compared for (R3)+(R4) and (R10)+(R11). The following rate constants overlap (and therefore cannot all be distinguished in the plots). (R3)+(R4): Stagni–Glarborg, (R10)+(R11): Stagni–Glarborg, (R6): Shrestha–Glarborg and Stagni–Otomo–Zhang, (R12): Shrestha–Glarborg–Otomo.

Recognizing that rate constant uncertainties vary greatly across reactions, the sensitivity coefficients for each reaction, $\partial\ln(X_i)/\partial\ln(k_j)$, shown in Fig. 5, were multiplied by their respective uncertainties, $\sigma\ln(k_j)$, to give uncertainty-weighted sensitivity coefficients (Fig. 6), which reflect the uncertainty in predictions of the mole fraction of a particular species i due to the uncertainty in the rate constant for reaction j. From this analysis, the reactions determining H_2NO formation ((R3) and, to a lesser extent, its competitive pathway (R4)) and consumption ((R6) and (R12)) notably emerged as the largest contributors to the uncertainty in model predictions for all species and at all temperatures except for 800 K (where predictions and measurements agree within uncertainties). Despite comparatively lower uncertainties in their rate constants, (R10) and (R11) still appear to be significant sources of uncertainty in predictions of both NH_3/NO_2 systems. However, (R1), which is also comparatively well studied [37,98–105], does not appear to be a significant source of prediction uncertainty here.

To provide further context regarding the uncertainties in the most influential reactions, the rate constants for (R3), (R4), (R6), (R10), (R11), and (R12) from the five models are compared with rate constants from theoretical calculations and experimental determinations in Fig. 7. (R3) and (R4), which are the major product channels for the NO_2 + NH_2 reaction, have been studied extensively in prior experiments [77, 106–117], yet there are few determinations and large differences in proposed expressions for the total rate constant ($k_{R3} + k_{R4}$) above ~700 K. Additionally, four of the five models assume that the branching ratio between (R3) and (R4), $k_{R4}/(k_{R3} + k_{R4})$, is independent of temperature, which disagrees with a recent theoretical study [117] and select experimental determinations [49,77,115].

(R10) and (R11), which are the major product channels for the NH_2 + NO reaction, are likely the most well studied reactions [109, 118–128] of all the influential reactions listed here (R1)–(R13). The experimental determinations of the branching ratio between (R10) and

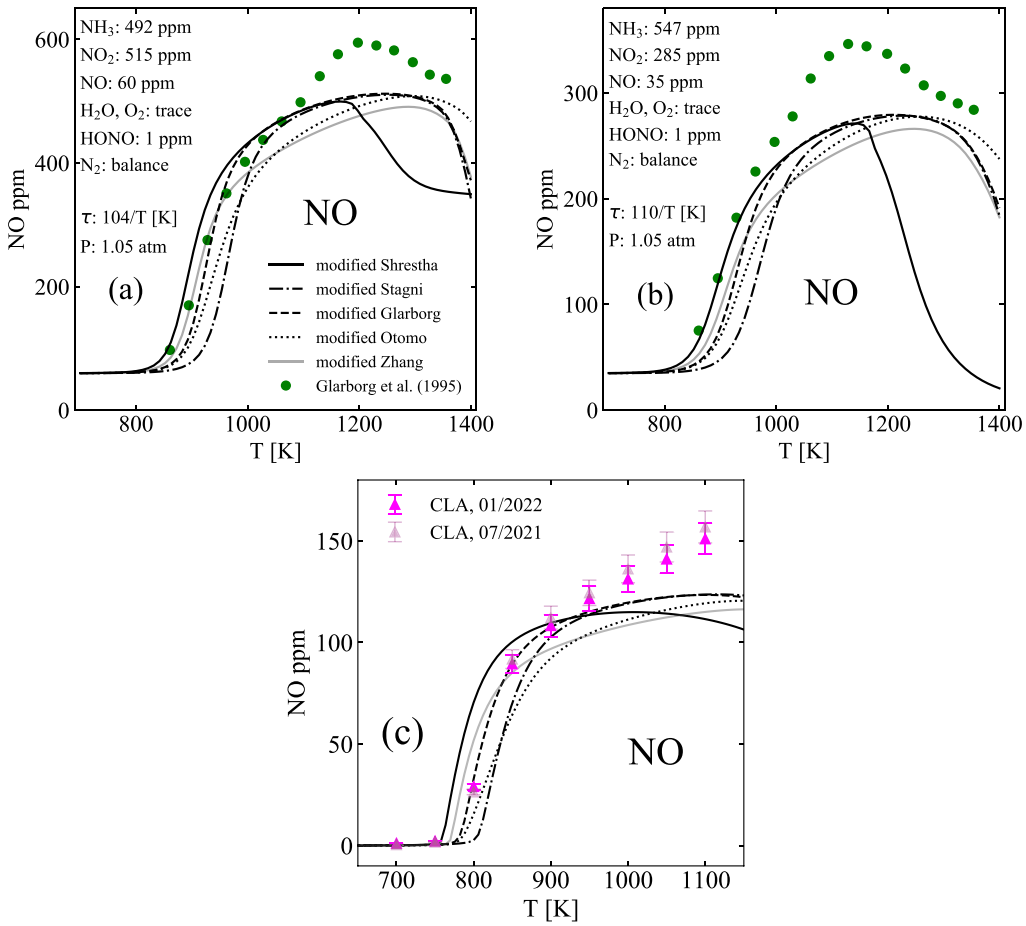

Fig. 8. Experimental measurements and modified model predictions of NO for the flow reactor experiments of Glarborg et al. [49] (a, b) and the present JSR experiments (c).

(R11), $k_{R11}/(k_{R10} + k_{R11})$, are very consistent and generally reproduced by rate expressions for most kinetic models, although the model of Shrestha et al. [60] gives a considerably larger ratio than the other models and the experimental determinations. Similar to the $k_{R3} + k_{R4}$ rate constant, however, there are few determinations and large differences in proposed expressions for the total rate constant ($k_{R10} + k_{R11}$) above ~950 K. While these uncertainties are smaller than other uncertainties present in the five models, deviations in the $k_{R10} + k_{R11}$ rate constant on the order of ~10% have significant influence over predictions of all major species.

In contrast to these comparatively well studied reactions, there is much greater variability among models for and much less is known about (R6) and (R12). All five models assume the rate constant for (R6) is equal to the rate constant for (R5) (NO_2 + HNO) since (R5) and (R6) have similar exothermicity. The models of Shrestha et al. and Glarborg et al. use a different rate constant for (R6) simply because they use an alternative rate constant for (R5) from Mebel et al. [89], who studied this reaction at the G2M(RCC,MP2) level. The rate constant for (R12) has also been highly uncertain. With the rate constants used by Shrestha et al., Glarborg et al., and Otomo et al. based on a single flash photolysis experiment [129] and the rate constants used by Stagni et al. and Zhang et al. based on estimates [10,97], the rate constants used by the five models span ~2-3 orders of magnitude over the JSR experimental temperature range shown in Fig. 7. Within the past few months, Stagni and Cavallotti [78] reported theoretical calculations of (R6) as part of a larger study on H-abstraction from H_2NO and Klippenstein and Glarborg [79,130] reported theoretical calculations of (R12) as part of a larger study of the $NH_2 + HO_2$ reaction. Notably, the calculations for (R6) [78] are one to two orders of magnitude slower at combustion-relevant temperatures than values in present models. Similarly, the calculations for (R12) [79,130], which are reasonably consistent with the only experimental determination at 300 K, show a negative temperature dependence not captured by any of the five models and yield rate constants at 1000 K roughly in the middle of the two-order-of-magnitude spread among the rate constants from different models.

Clearly, the significant uncertainties in several key reactions for the present system preclude any simple resolution of the discrepancies between the models and the experimental data. Naturally, one might wonder whether simply adopting theoretically calculated values (indicated by the blue lines in Fig. 7) for the branching ratio between (R3) and (R4) [117] (consistent with very recent modeling [77]) and rate constants for (R6) [78] and (R12) [79] would aid in resolving the discrepancies. Unfortunately, even with these changes in the rate constants for (R3), (R4), (R6), and (R12) implemented in each of the five models, none of the modified models reproduce the experimental measurements for all species (Figure S1 of the Supplemental Information). Of particular concern are the NO predictions as the modified models are unable to qualitatively reproduce the rise in NO with increasing temperature observed in both the previous plug flow reactor measurements of Glarborg et al. [49] (Fig. 8a,b) and the present JSR measurements (Fig. 8c).

Altogether, with such large uncertainties in several key reactions that are instrumental to the NH_3/NO_2 system and many other NH_3 oxidation systems (e.g. [37,51,52]) that are still not resolved by recent work on the key reactions [77–79], arriving at any definitive resolution of the discrepancies appears to require simultaneous consideration of multiple reactions and multiple data sets from both theory and experiment in a manner that considers the uncertainties of each.

5. Concluding remarks

Experimental measurements of NH_3, NO_2, NO, and O_2 were performed for a $NH_3/NO_2/O_2/N_2$ mixture over an intermediate temperature range (700–1100 K) in a jet-stirred reactor (JSR) to address gaps in previous validation data sets for ammonia oxidation via nitrogen-containing species. Comparisons of the experimental data against predictions from recent ammonia oxidation models show significant discrepancies, particularly for NH_3 and NO at elevated temperatures. Uncertainty-weighted sensitivity analysis identified that reactions controlling H_2NO formation ((R3) and its competitive pathway (R4)) and consumption ((R6) and (R12)) were among the largest contributors to uncertainty in the predictions and, consequently, among the most likely sources of the observed discrepancies. However, despite comparatively lower uncertainties in their rate constants, (R10) and (R11) were also found to contribute to model prediction uncertainties. These six key reactions for the NH_3/NO_2 system ((R3), (R4), (R6), (R10), (R11), and (R12)) are also known to be among the most important to predictions of many other H/N/O kinetic systems — notably NH_3 performance in combustion devices and NO_x reduction efficiencies in various combustion scenarios — and are therefore worthwhile candidates for improved rate constant quantification in future studies.

Altogether, with such large uncertainty contributions from several key reactions that are also instrumental to many other NH_3 oxidation systems, reliably unraveling the observed discrepancies in this system will require simultaneous consideration of many other H/N/O kinetic validation data sets to ensure the resulting model is truly comprehensive and sound. In that regard, we expect our ongoing implementation of the MultiScale Informatics approach [53,131–133] to an extensive set of experimental and theoretical data for H/N/O kinetics to be useful in resolving the discrepancies observed here in a manner consistent with other experimental and theoretical data and thereby establishing improved understanding of and models for ammonia.

Declaration of competing interest

The authors declare that they have no known competing financial interests or personal relationships that could have appeared to influence the work reported in this paper.

Data availability

Data will be made available on request.

Acknowledgments

The authors thank the Department of Defense Science, Mathematics, and Research for Transformation (SMART) program, the FY21/FY22 U.S. Army DEVCOM AC Environmental Quality Basic Research (EQBR) program, and the National Science Foundation Combustion and Fire Systems program (CBET-1944004) for funding and continued support.

Appendix A. Supplementary data

Supplementary material related to this article can be found online at https://doi.org/10.1016/j.jaecs.2022.100095.

Tabulated experimental data and rate constant uncertainty factors. Modeling analyses using other kinetic models.

References

[1] Erisman JW, Sutton MA, Galloway J, Klimont Z, Winiwarter W. How a century of ammonia synthesis changed the world. Nat Geosci 2008;1(10):636–9.
[2] Valera-Medina A, Xiao H, Owen-Jones M, David WI, Bowen P. Ammonia for power. Prog Energy Combust Sci 2018;69:63–102.
[3] Kobayashi H, Hayakawa A, Somarathne KKA, Okafor EC. Science and technology of ammonia combustion. Proc Combust Inst 2019;37(1):109–33.
[4] Valera-Medina A, Amer-Hatem F, Azad A, Dedoussi I, De Joannon M, Fernandes R, et al. Review on ammonia as a potential fuel: from synthesis to economics. Energy Fuels 2021;35(9):6964–7029.
[5] Herbinet O, Bartocci P, Dana AG. On the use of ammonia as a fuel-a perspective. Fuel Commun 2022;100064.
[6] Lyon RK. Method for the reduction of the concentration of NO in combustion effluents using ammonia. Tech. rep., 1975.
[7] Miller JA, Branch MC, Kee RJ. A chemical kinetic model for the selective reduction of nitric oxide by ammonia. Combust Flame 1981;43:81–98.
[8] Miller JA, Bowman CT. Mechanism and modeling of nitrogen chemistry in combustion. Prog Energy Combust Sci 1989;15(4):287–338.
[9] Hulgaard T, Dam-Johansen K. Homogeneous nitrous oxide formation and destruction under combustion conditions. AIChE J 1993;39(8):1342–54.
[10] Glarborg P, Dam-Johansen K, Miller JA, Kee RJ, Coltrin ME. Modeling the thermal $DeNO_x$ process in flow reactors. Surface effects and nitrous oxide formation. Int J Chem Kinet 1994;26(4):421–36.
[11] Glarborg P, Johnsson JE, Dam-Johansen K. Kinetics of homogeneous nitrous oxide decomposition. Combust Flame 1994;99(3–4):523–32.
[12] Kasuya F, Glarborg P, Johnsson JE, Dam-Johansen K. The thermal $DeNO_x$ process: Influence of partial pressures and temperature. Chem Eng Sci 1995;50(9):1455–66.
[13] Honorien J, Fournet R, Glaude P-A, Sirjean B. Theoretical study of the gas-phase thermal decomposition of urea. Proc Combust Inst 2021;38(1):355–64.
[14] Anderson WR, Meagher NE, Vanderhoff JA. Dark zones of solid propellant flames: Critically assessed datasets, quantitative model comparison, and detailed chemical analysis. Combust Flame 2011;158(7):1228–44.
[15] Chen C-C, McQuaid MJ. Mechanisms and kinetics for the thermal decomposition of 2-Azido-N,N-Dimethylethanamine (DMAZ). J Phys Chem A 2012;116(14):3561–76.
[16] Chen C-C, McQuaid M. A skeletal, gas phase, finite rate, chemical kinetics mechanism for modeling the deflagration of ammonium perchlorate-hydroxyl-terminated polybutadiene composite propellants. Tech. rep., US Army Research Laboratory Aberdeen Proving Ground United States; 2016.
[17] Samuels P, Spangler K, Iwaniuk D, Cornell R, Baker EL, Stiel LI. Detonation performance analyses for recent energetic molecules. In: AIP conference proceedings. Vol. 1979, (1):AIP Publishing LLC; 2018, 150033. http://dx.doi.org/10.1063/1.5044989.
[18] Cornell RE, LaGrotta CE, Barbet MC, Burke MP. Impact of chemically termolecular reactions on the kinetics of energetic materials. 2018 ESSCI spring technical meeting, 2018, p. 2B13.
[19] Cornell RE, Barbet MC, Burke MP. Influence of chemically termolecular reactions on species concentrations during RDX combustion. 11th U.S. national combustion meeting, 2019, p. 1A05.
[20] Cornell RE, Barbet MC, Burke MP. Experimentally testing the performance of small molecule chemistry relevant to energetic materials. 2020 ESSCI spring technical meeting, 2020, p. 2A07.
[21] Cornell RE, Barbet MC, Burke MP. Automated discovery of influential chemically termolecular reactions in energetic material combustion: A case study for RDX. Proc Combust Inst 2021;38(1):787–94. http://dx.doi.org/10.1016/j.proci.2020.06.354.
[22] Cornell RE, Barbet MC, Burke MP. An experimental and kinetic modeling study of NH_3 oxidation by NO_2 in a jet-stirred reactor. 2022 spring technical meeting of the eastern states section of the combustion institute, 2022, p. 3A05.
[23] Bernet N, Béline F. Challenges and innovations on biological treatment of livestock effluents. Bioresour Technol 2009;100(22):5431–6.
[24] Montes F, Meinen R, Dell C, Rotz A, Hristov AN, Oh J, et al. Special topics —- mitigation of methane and nitrous oxide emissions from animal operations: II. a review of manure management mitigation options. J Anim Sci 2013;91(11):5070–94.
[25] Hupa M, Karlström O, Vainio E. Biomass combustion technology development-it is all about chemical details. Proc Combust Inst 2017;36(1):113–34.
[26] Cornell RE, Barbet MC, Burke MP. Toward a more comprehensive understanding of the kinetics of a common biomass-derived impurity: NH_3 oxidation by N_2O in a jet-stirred reactor. Energy Fuels 2021;35(16):13338–48. http://dx.doi.org/10.1021/acs.energyfuels.1c01544.
[27] Ho PT, Townes CH. Interstellar ammonia. Annu Rev Astron Astrophys 1983;21(1):239–70.
[28] Randall DJ, Tsui T. Ammonia toxicity in fish. Mar Pollut Bull 2002;45(1–12):17–23.
[29] Felipo V, Butterworth RF. Neurobiology of ammonia. Progr Neurobiol 2002;67(4):259–79.

[30] Xiao H, Howard M, Valera-Medina A, Dooley S, Bowen PJ. Study on reduced chemical mechanisms of ammonia/methane combustion under gas turbine conditions. Energy Fuels 2016;30(10):8701–10.

[31] Xiao H, Valera-Medina A, Bowen PJ. Modeling combustion of ammonia/hydrogen fuel blends under gas turbine conditions. Energy Fuels 2017;31(8):8631–42.

[32] Mei B, Zhang X, Ma S, Cui M, Guo H, Cao Z, et al. Experimental and kinetic modeling investigation on the laminar flame propagation of ammonia under oxygen enrichment and elevated pressure conditions. Combust Flame 2019;210:236–46.

[33] Chiong M-C, Chong CT, Ng J-H, Mashruk S, Chong WWF, Samiran NA, et al. Advancements of combustion technologies in the ammonia-fuelled engines. Energy Convers Manage 2021;244:114460.

[34] Singh AS, Mohapatra S, Boyapati R, Elbaz AM, Dash SK, Roberts WL, et al. Chemical kinetic modeling of the autoignition properties of ammonia at low-intermediate temperature and high pressure using a newly proposed reaction mechanism. Energy Fuels 2021;35(16):13506–22.

[35] Glarborg P, Hashemi H, Marshall P. Challenges in kinetic modeling of ammonia pyrolysis. Fuel Commun 2022;100049.

[36] Abai AB, Zengel D, Janzer C, Maier L, Grunwaldt J-D, Olzmann M, et al. Effect of NO_2 on gas-phase reactions in lean $NO_x/NH_3/O_2/H_2O$ mixtures at conditions relevant for exhaust gas aftertreatment. Tech. rep., SAE Technical Paper; 2021.

[37] Stagni A, Cavallotti C, Arunthanayothin S, Song Y, Herbinet O, Battin-Leclerc F, et al. An experimental, theoretical and kinetic-modeling study of the gas-phase oxidation of ammonia. Reaction Chem Eng 2020;5(4):696–711. http://dx.doi.org/10.1039/C9RE00429G.

[38] Cañas JEC, Monge-Palacios M, Zhang X, Sarathy SM. Probing the gas-phase oxidation of ammonia: Addressing uncertainties with theoretical calculations. Combust Flame 2022;235:111708.

[39] Kumar P, Meyer TR. Experimental and modeling study of chemical-kinetics mechanisms for H_2-NH_3-air mixtures in laminar premixed jet flames. Fuel 2013;108:166–76.

[40] Song Y, Hashemi H, Christensen JM, Zou C, Marshall P, Glarborg P. Ammonia oxidation at high pressure and intermediate temperatures. Fuel 2016;181:358–65.

[41] Glarborg P, Miller JA, Ruscic B, Klippenstein SJ. Modeling nitrogen chemistry in combustion. Prog Energy Combust Sci 2018;67:31–68. http://dx.doi.org/10.1016/j.pecs.2018.01.002.

[42] Stagni A, Song Y, Olivier H, Fréderique B-L, Faravelli T, et al. An experimental and kinetic modeling study of NH_3 oxidation in a jet stirred reactor. In: 1st international conference on smart energy carriers. ITA; 2019, p. 1–4.

[43] Sabia P, Manna MV, Cavaliere A, Ragucci R, de Joannon M. Ammonia oxidation features in a jet stirred flow reactor. The role of NH_2 chemistry. Fuel 2020;276:118054.

[44] Li Y, Sarathy SM. Probing hydrogen-nitrogen chemistry: A theoretical study of important reactions in N_xH_y, HCN and HNCO oxidation. Int J Hydrogen Energy 2020;45(43):23624–37.

[45] Bertolino A, Fürst M, Stagni A, Frassoldati A, Pelucchi M, Cavallotti C, et al. An evolutionary, data-driven approach for mechanism optimization: theory and application to ammonia combustion. Combust Flame 2021;229:111366.

[46] Glarborg P, Kristensen PG, Dam-Johansen K, Alzueta M, Millera A, Bilbao R. Nitric oxide reduction by non-hydrocarbon fuels. Implications for reburning with gasification gases. Energy Fuels 2000;14(4):828–38.

[47] Mathieu O, Petersen EL. Experimental and modeling study on the high-temperature oxidation of Ammonia and related NO_x chemistry. Combust Flame 2015;162(3):554–70.

[48] Mei B, Ma S, Zhang X, Li Y. Characterizing ammonia and nitric oxide interaction with outwardly propagating spherical flame method. Proc Combust Inst 2021;38(2):2477–85.

[49] Glarborg P, Dam-Johansen K, Miller JA. The reaction of ammonia with nitrogen dioxide in a flow reactor: Implications for the NH_2 + NO2 reaction. Int J Chem Kinet 1995;27(12):1207–20.

[50] Wolfram P, Kyle P, Zhang X, Gkantonas S, Smith S. Using ammonia as a shipping fuel could disturb the nitrogen cycle. Nature Energy 2022. http://dx.doi.org/10.1038/s41560-022-01124-4.

[51] Song Y, Hashemi H, Christensen JM, Zou C, Marshall P, Glarborg P. Ammonia oxidation at high pressure and intermediate temperatures. Fuel 2016;181:358–65.

[52] Dai L, Gersen S, Glarborg P, Levinsky H, Mokhov A. Experimental and numerical analysis of the autoignition behavior of NH_3 and NH_3/H_2 mixtures at high pressure. Combust Flame 2020;215:134–44.

[53] Burke MP. Harnessing the combined power of theoretical and experimental data through multiscale informatics. Int J Chem Kinet 2016;48(4):212–35. http://dx.doi.org/10.1002/kin.20984.

[54] Barbet MC, Cornell RE, Burke MP. Coupling high throughput jet-stirred reactor experiments to experimental design algorithms: A step towards autonomous model development. 2022 spring technical meeting of the eastern states section of the combustion institute, 2022, p. 1C13.

[55] Herbinet O, Marquaire P-M, Battin-Leclerc F, Fournet R. Thermal decomposition of n-dodecane: Experiments and kinetic modeling. J Anal Appl Pyrol 2007;78(2):419–29.

[56] Herbinet O, Battin-Leclerc F. Progress in understanding low-temperature organic compound oxidation using a jet-stirred reactor. Int J Chem Kinet 2014;46(10):619–39.

[57] Ayass WW. Mixing in jet-stirred reactors with different geometries (Ph.D. thesis), 2013.

[58] Ayass WW, Nasir EF, Farooq A, Sarathy SM. Mixing-structure relationship in jet-stirred reactors. Chem Eng Res Des 2016;111:461–4.

[59] Azay P, Côme G-M. Temperature gradients in a continuous flow stirred tank reactor. Ind Eng Chem Process Des Dev 1979;18(4):754–6.

[60] Shrestha KP, Lhuillier C, Barbosa AA, Brequigny P, Contino F, Mounaïm-Rousselle C, et al. An experimental and modeling study of ammonia with enriched oxygen content and ammonia/hydrogen laminar flame speed at elevated pressure and temperature. Proc Combust Inst 2021;38(2):2163–74.

[61] Otomo J, Koshi M, Mitsumori T, Iwasaki H, Yamada K. Chemical kinetic modeling of ammonia oxidation with improved reaction mechanism for ammonia/air and ammonia/hydrogen/air combustion. Int J Hydrogen Energy 2018;43(5):3004–14.

[62] Zhang Y, Mathieu O, Petersen EL, Bourque G, Curran HJ. Assessing the predictions of a NO_x kinetic mechanism on recent hydrogen and syngas experimental data. Combust Flame 2017;182:122–41. http://dx.doi.org/10.1016/j.combustflame.2017.03.019.

[63] Kohse-Höinghaus K, Davidson DF, Chang AY, Hanson RK. Quantitative NH_2 concentration determination in shock tube laser-absorption experiments. J Quant Spectrosc Radiat Transfer 1989;42(1):1–17.

[64] Goodwin DG, Moffat HK, Speth RL. Cantera: an object-oriented software toolkit for chemical kinetics, thermodynamics, and transport processes. 2018, Version 2.4.059.

[65] Tsang W, Hampson R. Chemical kinetic data base for combustion chemistry. Part I. Methane and related compounds. J Phys Chem Ref Data 1986;15(3):1087–279.

[66] Tsang W. Chemical kinetic data base for combustion chemistry. Part 2. methanol. J Phys Chem Ref Data 1987;16(3):471–508.

[67] Tsang W. Chemical kinetic data base for combustion chemistry. Part 3: Propane. J Phys Chem Ref Data 1988;17(2):887–951.

[68] Tsang W. Chemical kinetic data base for combustion chemistry. Part 4. isobutane. J Phys Chem Ref Data 1990;19(1):1–68.

[69] Cohen N, Westberg K. Chemical kinetic data sheets for high-temperature reactions. Part II. J Phys Chem Ref Data 1991;20(6):1211–311.

[70] Tsang W. Chemical kinetic data base for combustion chemistry. Part V. Propene. J Phys Chem Ref Data 1991;20(2):221–73.

[71] Tsang W, Herron JT. Chemical kinetic data base for propellant combustion. I. Reactions involving NO, NO_2, HNO, HNO_2, HCN and N_2O. J Phys Chem Ref Data 1991;20(4):609–63.

[72] Tsang W. Chemical kinetic data base for propellant combustion. II. Reactions involving CN, NCO, and HNCO. J Phys Chem Ref Data 1992;21(4):753–91.

[73] Baulch D, Cobos C, Cox R, Esser C, Frank P, Just T, et al. Evaluated kinetic data for combustion modelling. J Phys Chem Ref Data 1992;21(3):411–734.

[74] Atkinson R, Baulch D, Cox RA, Crowley J, Hampson R, Hynes R, et al. Evaluated kinetic and photochemical data for atmospheric chemistry: Volume I - gas phase reactions of O_x, HO_x, NO_x and SO_x species. Atmos Chem Phys 2004;4(6):1461–738.

[75] Baulch D, Bowman C, Cobos CJ, Cox RA, Just T, Kerr J, et al. Evaluated kinetic data for combustion modeling: supplement II. J Phys Chem Ref Data 2005;34(3):757–1397.

[76] Smith GP, Tao Y, Wang H. Foundational fuel chemistry model version 1.0 (FFCM-1). 2016, URL http://nanoenergy.stanford.edu/ffcm1.

[77] Glarborg P. The $NH_3/NO_2/O_2$ system: Constraining key steps in ammonia ignition and N_2O formation. Combust Flame 2022;112311.

[78] Stagni A, Cavallotti C. H-abstractions by O_2, NO_2, NH_2, and HO_2 from H_2NO: theoretical study and implications for ammonia low-temperature kinetics. Proc Combust Inst 2022.

[79] Klippenstein SJ, Glarborg P. Theoretical kinetics predictions for NH_2 + HO_2. Combust Flame 2022;236:111787.

[80] Lovejoy E, Murrells T, Ravishankara A, Howard C. Oxidation of CS_2 by reaction with OH. II: Yields of HO_2 and SO_2 in oxygen. J Phys Chem 1990;94(6):2386–93.

[81] Koch TG, Sodeau JR. Photochemistry of nitric acid in low-temperature matrixes. J Phys Chem 1995;99(27):10824–9.

[82] Fulle D, Hamann H, Hippler H, Troe J. Temperature and pressure dependence of the addition reactions of HO to NO and to NO_2. IV. Saturated laser-induced fluorescence measurements up to 1400 bar. J Chem Phys 1998;108(13):5391–7.

[83] Chai J, Goldsmith CF. Rate coefficients for fuel+NO_2: Predictive kinetics for HONO and HNO_2 formation. Proc Combust Inst 2017;36(1):617–26. http://dx.doi.org/10.1016/j.proci.2016.06.133.

[84] Chen X, Fuller ME, Goldsmith CF. Decomposition kinetics for HONO and HNO_2. Reaction Chem Eng 2019;4(2):323–33.

[85] Fuller ME, Morsch P, Preußker M, Goldsmith CF, Heufer KA. The impact of NO_x addition on the ignition behaviour of n-pentane. Reaction Chem Eng 2021;6(11):2191–203.

[86] Mebel A, Diau E, Lin M-C, Morokuma K. Theoretical rate constants for the NH_3 + NO_x → NH_2 + HNO_x (x=1,2) reactions by ab initio MO/VTST calculations. J Phys Chem 1996;100(18):7517–25.

[87] Xu S, Lin M-C. Ab initio chemical kinetics for the NH_2 + HNO_x reactions, part I: kinetics and mechanism for NH_2 + HNO. Int J Chem Kinet 2009;41(11):667–77.

[88] Xu S, Lin M-C. Ab initio chemical kinetics for the NH_2 + HNO_x reactions, part II: kinetics and mechanism for NH_2 + HONO. Int J Chem Kinet 2009;41(11):678–88.

[89] Mebel A, Lin M-C, Morokuma K. Ab initio MO and TST calculations for the rate constant of the HNO + NO_2 → HONO + NO reaction. Int J Chem Kinet 1998;30(10):729–36.

[90] Glarborg P, Alzueta MU, Dam-Johansen K, Miller JA. Kinetic modeling of hydrocarbon/nitric oxide interactions in a flow reactor. Combust Flame 1998;115(1–2):1–27.

[91] Skreiberg Ø, Kilpinen P, Glarborg P. Ammonia chemistry below 1400 K under fuel-rich conditions in a flow reactor. Combust Flame 2004;136(4):501–18.

[92] Rasmussen CL, Hansen J, Marshall P, Glarborg P. Experimental measurements and kinetic modeling of $CO/H_2/O_2/NO_x$ conversion at high pressure. Int J Chem Kinet 2008;40(8):454–80.

[93] Michael J, Nava D, Payne W, Stief L. Absolute rate constants for the reaction of atomic hydrogen with ketene from 298 to 500 K. J Chem Phys 1979;70(11):5222–7.

[94] Ko T, Fontijn A. High-temperature photochemistry kinetics study of the reaction H + NO_2 → OH + NO from 296 to 760 K. J Phys Chem 1991;95(10):3984–7.

[95] Su M-C, Kumaran S, Lim K, Michael J, Wagner A, Harding L, et al. Rate constants, 1100 ≤ t ≤ 2000 k, for h + NO_2 → OH + NO using two shock tube techniques: Comparison of theory to experiment. J Phys Chem A 2002;106(36):8261–70.

[96] Burkholder JB, Mellouki A, Talukdar R, Ravishankara A. Rate coefficients for the reaction of OH with HONO between 298 and 373 K. Int J Chem Kinet 1992;24(8):711–25.

[97] Dean AM, Bozzelli JW. Combustion chemistry of nitrogen. In: Gas-phase combustion chemistry. Springer; 2000, p. 125–341.

[98] Perry R, Atkinson R, Pitts Jr. J. Rate constants for the reactions OH + H_2S → H_2O + SH and OH + NH_3 → H_2O + NH_2 over the temperature range 297-427 K. J Chem Phys 1976;64(8):3237–9.

[99] Silver JA, Kolb CE. Rate constant for the reaction NH_3 + OH → NH_2 + H2O over a wide temperature range. Chem Phys Lett 1980;75(1):191–5.

[100] Salimian S, Hanson R, Kruger C. High temperature study of the reactions of O and OH with NH_3. Int J Chem Kinet 1984;16(6):725–39.

[101] Stephens RD. Absolute rate constants for the reaction of hydroxyl radicals with ammonia from 297 to 364 K. J Phys Chem 1984;88(15):3308–13.

[102] Zabielski M, Seery D. High temperature measurements of the rate of the reaction of OH with NH_3. Int J Chem Kinet 1985;17(11):1191–9.

[103] Jeffries J, Smith G. Kinetics of the reaction OH + NH_3. Chemischer Informationsdienst 1986;17(21):no–no.

[104] Diau EWG, Tso TL, Lee YP. Kinetics of the reaction hydroxyl + ammonia in the range 273-433 K. J Phys Chem 1990;94(13):5261–5.

[105] Nguyen TL, Stanton JF. High-level theoretical study of the reaction between hydroxyl and ammonia: Accurate rate constants from 200 to 2500 K. J Chem Phys 2017;147(15):152704.

[106] Bedford G, Thomas J. Reaction between ammonia and nitrogen dioxide. J Chem Soc Faraday Trans I 1972;68:2163–70.

[107] Hack W, Schacke H, Schröter M, Wagner HG. Reaction rates of NH_2-radicals with NO, NO_2, C_2H_2, C_2H_4 and other hydrocarbons. In: Symposium (international) on combustion. Vol. 17, (1):Elsevier; 1979, p. 505–13.

[108] Kurasawa H, Lesclaux R. Kinetics of the reaction of NH_2 with NO_2. Chem Phys Lett 1979;66(3):602–7.

[109] Bulatov V, Ioffe A, Lozovsky V, Sarkisov O. On the reaction of the NH_2 radical with NO at 295-620 K. Chem Phys Lett 1989;161(2):141–6.

[110] Meunier H, Pagsberg P, Sillesen A. Kinetics and branching ratios of the reactions NH_2 + NO_2 → N_2O + H_2O and NH_2 + NO_2 → H_2NO + NO studied by pulse radiolysis combined with time-resolved infrared diode laser spectroscopy. Chem Phys Lett 1996;261(3):277–82.

[111] Quandt RW, Hershberger JF. Diode laser study of the product branching ratio of the NH_2 (X^2B_1) + NO_2 reaction. J Phys Chem 1996;100(22):9407–11.

[112] Park J, Lin M-C. Mass-spectrometric determination of product branching probabilities for the NH_2 + NO_2 reaction at temperatures between 300 and 990 K. Int J Chem Kinet 1996;28(12):879–83.

[113] Park J, Lin M-C. A mass spectrometric study of the NH_2 + NO2 reaction. J Phys Chem A 1997;101(14):2643–7.

[114] Lindholm N, Hershberger JF. Product branching ratios of the NH_2 (X^2B_1) + NO_2 reaction. J Phys Chem A 1997;101(27):4991–5.

[115] Song S, Golden D, Hanson R, Bowman C. A shock tube study of the NH_2 + NO_2 reaction. Proc Combust Inst 2002;29(2):2163–70.

[116] Song S, Golden DM, Hanson RK, Bowman CT. A shock tube study of benzylamine decomposition: overall rate coefficient and heat of formation of the benzyl radical. J Phys Chem A 2002;106(25):6094–8.

[117] Klippenstein SJ, Harding LB, Glarborg P, Gao Y, Hu H, Marshall P. Rate constant and branching fraction for the NH_2 + NO_2 reaction. J Phys Chem A 2013;117(37):9011–22.

[118] Stief LJ, Brobst WD, Nava DF, Borkowski RP, Michael JV. Rate constant for the reaction NH_2 + NO from 216 to 480 k. J Chem Soc Faraday Trans II 1982;78(8):1391–401.

[119] Silver JA, Kolb CE. Kinetic measurements for the reaction of amidogen + nitric oxide over the temperature range 294-1215 K. J Phys Chem 1982;86(16):3240–6.

[120] Atakan B, Jacobs A, Wahl M, Weller R, Wolfrum J. Kinetic measurements and product branching ratio for the reaction NH_2 + NO at 294-1027 K. Chem Phys Lett 1989;155(6):609–13.

[121] Wolf M, Yang DL, Durant JL. Kinetic studies of NH_x radical reactions. J Photochem Photobiol A: Chemistry 1994;80(1–3):85–93.

[122] Park J, Lin M-C. Direct determination of product branching for the NH_2 + NO reaction at temperatures between 302 and 1060 K. J Phys Chem 1996;100(9):3317–9.

[123] Glarborg P, Kristensen PG, Dam-Johansen K, Miller JA. Branching fraction of the NH_2 + NO reaction between 1210 and 1370 K. J Phys Chem A 1997;101(20):3741–5.

[124] Park J, Lin M-C. Laser-initiated NO reduction by NH_3: Total rate constant and product branching ratio measurements for the NH_2 + NO reaction. J Phys Chem A 1997;101(1):5–13.

[125] Wolf M, Yang D, Durant J. A comprehensive study of the reaction NH_2 + NO → products: reaction rate coefficients, product branching fractions, and ab initio calculations. J Phys Chem A 1997;101(35):6243–51.

[126] Park J, Lin M. Product branching ratios in the NH_2 + NO reaction: a re-evaluation. J Phys Chem A 1999;103(44):8906–7.

[127] Song S, Hanson R, Bowman C, Golden D. Shock tube determination of the overall rate of NH_2 + NO → products in the thermal De-NO_x temperature window. Int J Chem Kinet 2001;33(11):715–21.

[128] Song S, Hanson RK, Bowman CT, Golden DM. A shock tube study of the product branching ratio of the NH_2 + NO reaction at high temperatures. J Phys Chem A 2002;106(40):9233–5.

[129] Sun F, DeSain J, Scott G, Hung P, Thompson R, Glass G, et al. Reactions of NH_2 with NO_2 and of OH with NH_2O. J Phys Chem A 2001;105(25):6121–8.

[130] Glarborg P, Hashemi H, Cheskis S, Jasper AW. On the rate constant for NH_2 + HO2 and third-body collision efficiencies for NH_2 + H (+ M) and NH_2 + NH_2 (+ M). J Phys Chem A 2021;125(7):1505–16.

[131] Burke MP, Klippenstein SJ, Harding LB. A quantitative explanation for the apparent anomalous temperature dependence of OH + HO_2=H_2O + O_2 through multi-scale modeling. Proc Combust Inst 2013;34(1):547–55. http://dx.doi.org/10.1016/j.proci.2012.05.041.

[132] Burke MP, Goldsmith CF, Klippenstein SJ, Welz O, Huang H, Antonov IO, et al. Multiscale informatics for low-temperature propane oxidation: Further complexities in studies of complex reactions. J Phys Chem A 2015;119(28):7095–115.

[133] LaGrotta CE, Barbet MC, Lei L, Burke MP. Towards a high-accuracy kinetic database informed by theoretical and experimental data: CH_3 + HO_2 as a case study. Proc Combust Inst 2021;38(1):1043–51. http://dx.doi.org/10.1016/j.proci.2020.06.324.